Magnetism of nanostructures studied by x-ray magnetic circular dichroism: Fe on Cu(111)

P. Ohresser, G. Ghiringhelli, O. Tjernberg, and N. B. Brookes
European Synchrotron Radiation Facility, BP 220, F-38043 Grenoble, France

M. Finazzi
TASC-INFM, Elettra Synchrotron Light Source, Strada Statale 14, Km. 163.5, 34012 Basovizza, Trieste, Italy
(Received 26 January 2000; revised manuscript received 10 May 2000)

Epitaxial growth of Fe on a stepped Cu(111) surface leads to the formation of fcc Fe stripes along the step edges for coverages lower than 1.5 monolayer (ML). Using the sensitivity of the x-ray magnetic circular dichroism and sum-rule analysis, the changes in the magnetic properties in the low thickness range from ~5% of a monolayer to 4 ML, covering the one-dimensional (1D) coalescence (~0.8 ML) and the 2D percolation limit (~1.5 ML), have been determined. The determination of the spin moment (m_{spin}) indicates significant features which can be correlated to the morphological transition. In particular, the m_{spin} decreases at the 1D coalescence limit, but increases as the film reaches the 2D percolation limit and starts to transform into the bcc phase. This behavior is tentatively ascribed to the decrease in the Fe atomic volume, as it is well known that such changes can dramatically modify the magnetic properties of γ-Fe.

I. INTRODUCTION

The constant demand for higher storage density in the magnetic device industry has resulted in an increasing interest in nanostructures. In order to produce nanoparticles with high magnetization and stable properties, the basic physics of these particles needs to be understood. In this context we have studied Fe nanostructures obtained by taking advantage of the self-organization of Fe on Cu(111).

In recent years, many investigations have been made on the structural and magnetic properties of face-centered-cubic (fcc) γ-Fe films grown on a Cu substrate. This interest is mainly due to the fact that the Cu substrate allows the fcc phase of Fe to be stabilized at room temperature (RT), whereas for bulk fcc Fe this phase only appears at a temperature in excess of 1186 K, which is above the Curie temperature. The majority of this work was more concerned with the properties of the two-dimensional (2D) Fe films.[1] However, taking advantage of the decoration effect of Fe growth on Cu(111), Shen *et al.* have recently managed to produce 1D Fe stripes on a stepped Cu(111) substrate.[2,3] It has been found, by scanning tunneling microscopy (STM), that in the submonolayer range the deposited Fe atoms form parallel stripes along the step edges (step decoration). The magnetism of the stripes has a superparamagnetic nature that is distinguished from that of a 2D ferromagnetic film mainly by its time-dependent remanent magnetization. At variance with what one would expect, no in-line anisotropy due to the spin-orbit interaction has been observed.[4] Actually, above ~0.3 ML [the lowest coverage investigated by the magneto-optical Kerr effect (MOKE) measurements of Refs. 2 and 3], Fe films behave similarly to films grown on Cu(111), with an out-of-plane magnetic anisotropy until the bcc phase transformation occurs at ~2.5–3 ML.

The aim of the present study is to obtain a comprehensive understanding of the magnetism of nanoscale Fe structures deposited on a vicinal Cu(111) [Cu(111)-vic] substrate. Going from a few percent of a monolayer to 4 ML, we cover the whole thickness range of interest for γ-Fe. In particular, below 0.8 ML, Fe essentially forms clusters of low spatial extension (fewer than 3000 atoms per cluster), while in the coverage range from 0.8 ML to ~1.5 ML, Fe forms 1D stripes (1–2 ML high) whose width increases with coverage until the 2D percolation occurs (~1.5 ML). These results, on the growth morphology, come from the STM experiments of Refs. 2 and 3. Two different kinds of effects are expected: the size effects due to the more atomiclike behavior and low dimensionality of such nanostructures, and the structural effects. Indeed, an interesting feature of γ-Fe is that its magnetic structure strongly depends on its lattice constant. Generally, for γ-Fe theoretical models predict a larger magnetic moment per atom as well as ferromagnetic ordering as the lattice parameter is increased.[5–7] However, low-spin ferromagnetism, nonmagnetic, and antiferromagnetic phases are also predicted.[5–7] Until now, there has been little experimental evidence for the existence of different ferromagnetic γ-Fe phases. For instance, in Refs. 8 and 9 the authors demonstrate the possibility of growing γ-Fe on Cu(111) in a high-spin phase (with a total magnetic moment close to $2.2\mu_B$ per atom) using pulsed laser deposition (PLD) while the films obtained using thermal deposition (TD) give a low-spin phase. The different magnetic properties are explained by the different film morphologies and structures induced by the different growth kinetics involved with these two techniques: layer by layer for PLD and 3D growth for TD. From this experiment it appears that very small changes in the lattice parameters can indeed lead to different magnetic properties and that such small structural changes can be expected at low coverage, for instance at the 1D coalescence.[10]

This is not exactly the case for the system Fe/Cu(100) where a high-spin phase is also observed in the γ-Fe thickness range, but is associated to a tetragonal expansion leading to a fct phase rather than to a fcc structure.[11] Indeed, up to 4 ML, a high-spin phase is observed in correlation with the fct structure. The spin moment is confined to a range between $\sim 2.3\mu_B$ and $\sim 3.3\mu_B$ according to different x-ray

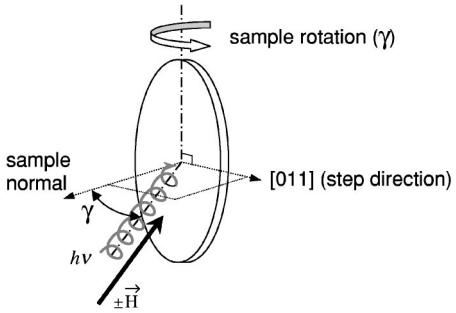

FIG. 1. Scheme of the geometry of the experimental setup. The magnetic field is aligned with the direction of the light. γ (obtained by rotating the sample) is the angle between the magnetic field and the normal to the sample surface. When $\gamma=0$, the light is along the sample normal. The direction of the monatomic steps on the Cu(111) substrate is also indicated.

magnetic circular dichroism (XMCD) measurements.[12] Above 4 ML, a phase transformation takes place and only the two first planes are still fct while the rest of the film becomes fcc. At correspondence with this phase transition, the net magnetization decreases and then remains constant until the bcc phase transformation occurs around 11 ML.[11]

These different experimental results illustrate the complexity of accurately determining thin-film magnetic moments and show the importance of utilizing a very sensitive probe. In this context, XMCD appears to be a well-suited tool. Indeed, aside from its element specificity, its high sensitivity makes it ideal to study submonolayer-thick Fe films. Moreover, with the help of sum rules XMCD allows a quantitative determination of the spin (m_{spin}) and the orbital (m_{orb}) magnetic moments.[13,14] We have obtained these quantities for nanoscale Fe clusters and 1D Fe stripes. As shown below, our measurements confirm the out-of-plane magnetic anisotropy for very low coverages and show the existence of two low-spin phases with different spin moments: $\sim 1.4\mu_B$ below 0.8 ML and $0.6\mu_B$ above, before the film undergoes its fcc to bcc phase transformation.

II. EXPERIMENT

The measurements were performed at beamline ID12B of the European Synchrotron Radiation Facility in Grenoble, using 90% circularly polarized light from a helical undulator. The magnetic characterization and the thin-film growth were performed *in situ* in an ultrahigh-vacuum 7 T superconducting magnet chamber with a vacuum better than 5×10^{-11} mbar and a temperature range going from 6 to 320 K. The applied magnetic field is aligned with the photon propagation vector and spin direction, as shown in Fig. 1. By rotating the sample by an angle γ (see Fig. 1), we can magnetize the sample from perpendicular to in-plane geometry allowing angular-dependent measurements. The sample preparation, consisting of cycles of Ar^+ sputtering and annealing at 700 K, was done in an independent chamber. Once clean, the sample was transferred, without breaking the vacuum, to the main chamber for Fe deposition and analysis.

The copper substrate had a miscut of 1.2° with respect to the (111) orientation. The surface steps were aligned along the [011] direction with a (001) microfacet. The average terrace width is about 10 nm. The crystallographic quality of the sample was checked with low-energy electron diffraction which exhibited the sharp $p(1\times1)$ pattern. The morphology of the surface was checked *ex situ* using an atomic-force microscopy in air. Although this technique does not enable characterization with good atomic resolution, it is sufficient to check the film's step morphology. The Fe films were prepared in the analysis chamber from an iron wire (4 N purity) heated by *e*-beam bombardment. The sample was kept at 280 K to minimize interdiffusion processes.[15] During the measurements, the temperature was always below RT. The Fe thickness was deduced from the Fe edge jump. The validity of this method was preliminarily tested with Fe films calibrated with Auger electron spectroscopy, low-energy electron diffraction (LEED), medium-energy electron diffraction (leading to amplitude oscillations of the specular beam with the filling of each layer in a similar way to reflection high-energy electron diffraction experiments[16]), and checked with a quartz microbalance. The LEED allowed us to confirm the critical thickness of the fcc to bcc structural transition (~2.5 ML). The consistency of our overall thickness calibration was further confirmed by the determination of the Curie temperature (T_C) and of the blocking temperature (T_B) of our films for the lower coverages as we will demonstrate in the next section.

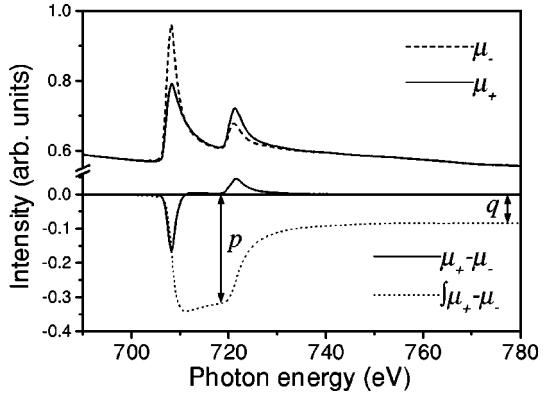

FIG. 2. Typical XMCD spectra for a coverage of 0.13 ML of Fe/Cu(111)-vic (total electron yield mode). μ_+ and μ_- correspond, respectively, to the absorption of left and right helicity (taking the direction of the magnetic field as the quantization axis). This measurement has been done at normal incidence ($\gamma=0°$), $T=20$ K and $H=\pm4$ T. The variables p and q on the integral of the XMCD signal indicate the values used in the sum rules (see text).

Our XMCD measurements are based on the circular magnetic dichroism at the Fe $L_{2,3}$ absorption edges. When the photon energy is swept across the spin-orbit-split L_3 and L_2 edges, core electrons are excited into unoccupied $3d$ valence states. The spin conservation in the absorption process aligns the spin of the $2p$ core hole with that of the empty $3d$ orbitals. Strong spin-orbit coupling in the core shell leads to an x-ray-absorption spectroscopy (XAS) signal which depends on the relative alignment of photon spin and sample magnetization. This can be seen in Fig. 2, where typical XAS spectra are shown for a Fe coverage of 0.13 ML. The spectra were obtained at normal incidence by reversing the direction of the magnetic field ($H=\pm4$ T). The XAS spectra were taken by measuring both the total electron yield and the total

fluorescence yield (detected at 90° to incident beam), although only the former is generally directly proportional to the absorption cross section.[17] The XMCD spectrum is the difference between the two XAS spectra recorded with opposite orientation of the magnetic field and the helicity of the light, which we will call μ_+ and μ_- for simplicity. $\mu_+(\mu_-)$ corresponds to the absorption coefficient of left (right) circularly polarized light taking the direction of the magnetic field as the quantization axis. Two important magneto-optical sum rules have been derived to deduce the orbital and spin magnetic moment from the XMCD.[13,14] Using the same notation as Ref. 18, we can write for the $L_{2,3}$ edges

$$m_{\mathrm{orb}}=\frac{-4qN_h}{3r}, \tag{1}$$

$$m_{\mathrm{spin}}^{\mathrm{eff}}=\frac{-(6p-4q)N_h}{r}, \tag{2}$$

where p and q are, respectively, the integral over L_3 and over (L_3+L_2) of the XMCD signal (given by $\mu_+-\mu_-$), r is the integral of the ''white line'' intensity of the magnetization averaged absorption cross section $(\mu_++\mu_-)$ (to separate the ''white line'' from the continuum, a simple steplike function was subtracted[19]), and N_h is the number of holes in the $3d$ band. $m_{\mathrm{spin}}^{\mathrm{eff}}$ counts for the effective magnetic spin moment as it includes a dipolar term m_T describing the anisotropy of the spin moment: $m_{\mathrm{spin}}^{\mathrm{eff}}=m_s+7m_T$. In practice, one should correct the data for saturation effects which can introduce some artifacts, but as we are working with very low coverage (below 4 ML) these corrections are negligible.[20] N_h is in principle unknown although it can be estimated from band-structure calculations. In the case of bcc Fe, a value close to 3.39 is found to give good agreement between theory and experiment.[18] However, since we are only interested in very small fcc structures, we will mostly consider magnetic moment per hole, i.e., m_{orb}/N_h and $m_{\mathrm{spin}}^{\mathrm{eff}}/N_h$.[21]

III. SAMPLE CHARACTERIZATION AND DATA TREATMENT

To make sure that we have reproduced the film morphology of the previous experiment by Shen *et al.*,[2,3] we compare some magnetic critical parameters such as T_C and T_B. Below the 2D percolation, the Fe/Cu(111) system is characterized by a superparamagnetic phase. This magnetic phase is like a paramagnetic one, except that the basic element is a spin block with parallel spins alignment and is thus a giant magnetic moment, and due to thermal activation there is no long-range order. T_C corresponds to the disappearance of the magnetic ordering inside each block, and T_B, which is particular to the superparamagnetic phase, can be defined as the temperature below which the anisotropy barrier between opposite magnetization directions cannot be exceeded by thermal spin fluctuations. A preferred spin direction is then selected by an external field, leading to a nonzero remanent macroscopic sample magnetization. However, in contrast to ferromagnetism, this remanence decays in time, with a time scale depending on the temperature. Both T_C and T_B are characteristic of the coverage and morphology and can easily be estimated from the magnetization curve: the former by the vanishing of the magnetization at saturation ($T>T_C$, Fig. 3, top curve) and the latter by the appearance of remanence ($T<T_B$, Fig. 3, bottom curve).

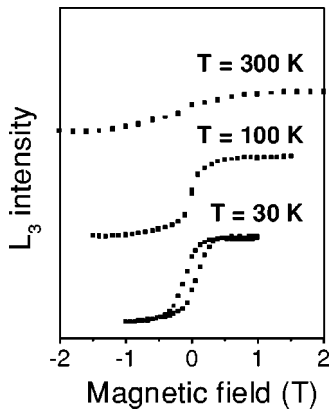

FIG. 3. Magnetization curves at different temperatures for a coverage of 0.6 ML Fe/Cu(111)-vic. At $T=30$ K we observe a remanence which indicates that we are below the blocking temperature, and at $T=300$ K the saturation has already dropped, implying that we are just above T_C.

The magnetization curve is obtained by monitoring the intensity of the L_3 absorption edge as a function of the applied magnetic field.[22,23] The results for 0.6 ML Fe/Cu(111) at three different temperatures are shown in Fig. 3. The three phases are clearly seen and for this particular coverage we estimate $T_C\approx(280\pm20)$ K and $T_B\approx(80\pm20)$ K. Another parameter which can be deduced from the magnetization curves, in the superparamagnetic phase, is the cluster size. Indeed, it has been shown in several experiments on Co clusters deposited on a Au(111) substrate[22,24,25] that a fit with a Langevin function of the magnetization,

$$M(H)\propto\coth\left(\frac{mN_{\mathrm{at}}H}{kT}\right)-\left(\frac{mN_{\mathrm{at}}H}{kT}\right)^{-1}, \tag{3}$$

where N_{at} is the average number of atoms per cluster, m is the magnetic moment per atom, and k is the Boltzmann's constant, can give satisfactory results for $T_B<T<T_C$. The magnetic moment per atom is deduced from the sum rules as explained in the next section ($m=m_{\mathrm{spin}}+m_{\mathrm{orb}}$). One still needs to be cautious with this method, as in the case of a nonuniform size distribution it tends to overestimate the average cluster size as demonstrated by STM in Ref. 25. Once the clusters have coalesced to form 1D stripes, spin blocks are formed with dimensions smaller than the actual size of the structure, demanding a more complex description.[2] As in our case we do not have a regular distribution, either in size or in patterning, we will only use this method to obtain an order of magnitude of the average number of atoms N_{at} per cluster and only for the thickness range below the 1D coalescence.

In Fig. 4, we show the parameters T_C, T_B, and N_{at} deduced from our experiment (solid symbols) and from Refs. 2 and 3 (open symbols). The good agreement between the two sets of data, for similar experimental conditions (evaporation rate, vacuum, magnetic-field sweeping rate etc.), confirms that we are growing Fe nanostructures with a similar morphology to those studied by Shen *et al.*[2,3] The expected de-

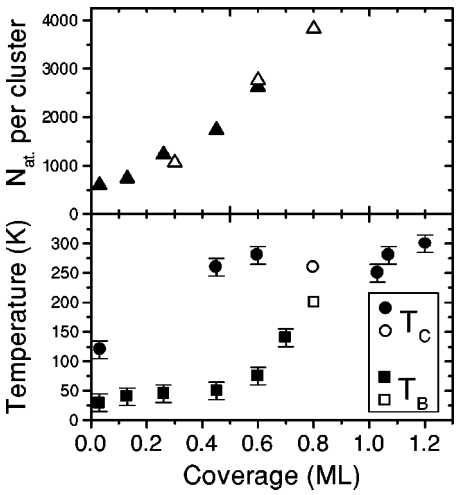

FIG. 4. Curie temperature (circles), blocking temperature (squares), and average number of atoms per cluster (triangles) as a function of the coverage. The open symbols correspond to similar measurement done by Shen *et al.* in Refs. 2 and 3.

crease of T_B is now measured down to very low coverages, resulting in a value of T_B equal to $30\,\mathrm{K}^{+20\,\mathrm{K}}_{-10\,\mathrm{K}}$ for the lowest coverage at (0.03 ± 0.01) ML. These measurements confirm the observation made by Shen *et al.* that for coverage below 0.3 ML T_B should be below 50 K. This behavior means a reduction of the absolute height of the anisotropy barrier, but actually the anisotropy energy per atom $E_A \propto kT_B/N_{\mathrm{at}}$ increases[22] (because the decrease of T_B is slower than the decrease of N_{at}) when the cluster size is reduced, i.e., at low coverages. This increase is further underlined by the angle-dependent XMCD, taken below T_B and obtained with a magnetic field sufficient to fully saturate the sample, which allows a determination of the anisotropy of m_{orb}.

For each film the incidence angle γ, i.e., the angle between the incident light and the surface normal, was varied from 0° to 60° in 15° steps, with the rotation axis being perpendicular to the step direction (see the scheme of Fig. 1). At each angle we applied the sum rules on the measured XMCD spectra and systematically found larger values for the orbital moment at normal incidence compared to grazing incidence ($\gamma=60°$). According to Refs. 2 and 3, no magnetic anisotropy was observed in the longitudinal geometry by MOKE. For very low coverage (below 0.3 ML), we can reasonably assume the same since for these coverages the steps do not break the symmetry and the Fe film has the fcc(111) symmetry. Assuming uniaxial anisotropy,[2,3] we can compare our experimental data with the model of Bruno,[26] who suggests that, for a completely filled majority band, the $3d$ orbital magnetic moment varies (at the lowest order) as

$$m^{\gamma}_{\mathrm{orb}} = m^{\perp}_{\mathrm{orb}} + (m^{\parallel}_{\mathrm{orb}} - m^{\perp}_{\mathrm{orb}})\sin^2\gamma, \qquad (4)$$

where $m^{\gamma}_{\mathrm{orb}}$ denotes the orbital magnetic moment measured at the angle γ, and $m^{\perp}_{\mathrm{orb}}$ and $m^{\parallel}_{\mathrm{orb}}$ are, respectively, the orbital magnetic moments measured perpendicular and parallel to the easy axis of magnetization. Figure 5 shows the good agreement between our experiment at 0.13 ML of Fe and the theoretical prediction. The anisotropy of the film, characterized by $m^{\perp}_{\mathrm{orb}} - m^{\parallel}_{\mathrm{orb}}$, has the same qualitative behavior as the anisotropy energy per atom E_A, i.e., it increases at very low

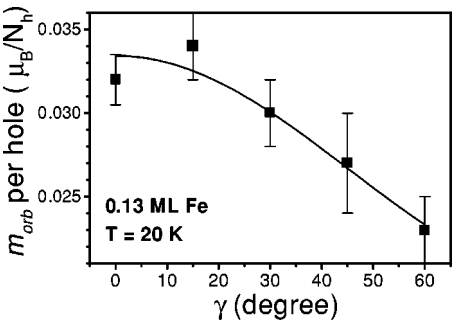

FIG. 5. $3d$ orbital magnetic moment per hole, measured on 0.13 ML of Fe deposited on the vicinal Cu(111) substrate, as a function of the incidence angle γ. ($H=4$ T, $T=20$ K). The solid curve is a fit using the model of Bruno (see text for details). The fit gives $m^{\perp}_{\mathrm{orb}}=(0.032\pm0.003)\mu_B$/hole and $(m^{\perp}_{\mathrm{orb}}-m^{\parallel}_{\mathrm{orb}})=(0.013\pm0.003)\mu_B$/hole. (The measurement has been performed below the blocking temperature with a magnetic field sufficient to saturate the sample).

coverage. This phenomenon, discussed later, is correlated to the increase of the orbital moment as the film's nominal thickness is reduced and the film becomes more atomiclike (Fig. 6). The increase of the scattering of the m_{orb} data at very low coverages is due to the higher sensitivity of this variable to any experimental noise as compared to m_{spin}. Indeed, as seen in the sum rules [Eqs. (1) and (2)], m_{orb} only depends on q, which is the integral of the XMCD signal over the L_3 and L_2 edges, while m_{spin} is dominated by p, which results only from the integral over the L_3 edge.

Figure 6 shows the variation of m_{orb}/N_h and m_{spin}/N_h with the coverage. To derive m_{spin}/N_h we have to isolate in $m^{\mathrm{eff}}_{\mathrm{spin}}/N_h$ the contribution from the magnetic dipole term m_T. This term arises from the anisotropy of the spin density within the Wigner-Seitz cell[14] and therefore could represent

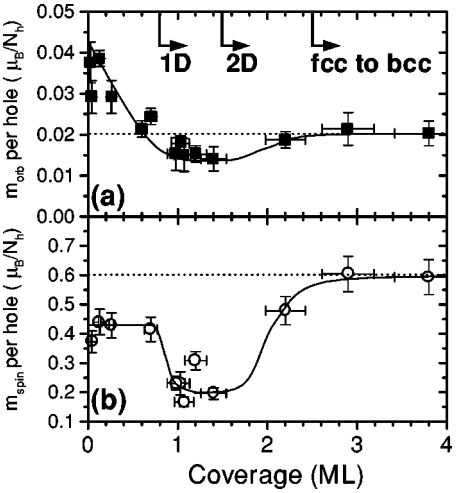

FIG. 6. Orbital (a) and spin magnetic moment (b) per hole as a function of coverage. The solid lines are guides for the eye. The dashed lines correspond to the values for the magnetic moment commonly accepted for bulk bcc Fe. The arrows on the top scale at 0.8, 1.5, and 2.5 ML correspond, respectively, to the approximate coverage where the Fe starts to coalesce into 1D wire, reaches the 2D percolation, and undergoes the fcc to bcc phase transformation. (All the measurements have been performed below the blocking temperature with a magnetic field sufficient to saturate the sample.)

a significant contribution for a low-symmetry crystal environment or a large spin-orbit splitting in the valence band.[27] In our case, the cluster morphology is likely to lead to nonnegligible values for m_T. Hence, we follow the arguments of Stöhr and König developed in Ref. 28. They demonstrate that for $3d$ metals the effect of spin-orbit coupling on the magnetic dipolar term is weak and the spin moment is isotropic to a very good approximation. Therefore, in the case of uniaxial anisotropy we have $m_T^{\parallel}+2m_T^{\perp}=0$ and since m_T^{γ} is expected to vary similarly to the orbital moment, i.e.,

$$m_T^{\gamma}=m_T^{\perp}+(m_T^{\parallel}-m_T^{\perp})\sin^2\gamma, \tag{5}$$

we can write

$$m_{\text{eff-spin}}^{\gamma}=(m_{\text{spin}}-7m_T^{\perp})+\tfrac{21}{2}m_T^{\perp}\sin^2\gamma. \tag{6}$$

This relation allows us to derive for each coverage the contribution of the spin moment plotted in Fig. 6.

As already stated in the Introduction, the Fe film undergoes a phase transition from fcc to bcc around 2.5–3 ML. Actually, bcc nucleation can appear early in the growth, but only dominates above a coverage of 2.5 ML.[3,9] This structural phase transition is evident in Fig. 6 by the increase of both m_{orb}/N_h and m_{spin}/N_h above 1.6–1.8 ML. Indeed as bcc Fe is expected to have larger moments than our measured values at ~1.5 ML, this increase only means that the bcc parts contribute more and more to the magnetic signal until the film is fully transformed (around 3 ML), where the magnetic moments reach the common values for the bulk bcc Fe, i.e., $m_{\text{spin}}/N_h=0.58\mu_B$ and $m_{\text{orb}}/N_h=0.02\mu_B$.[18] A similar behavior is seen using MOKE measurements for the case of Fe on a flat Cu(111) substrate. Nevertheless, the most intriguing feature in Fig. 6 is the clear decrease of the spin magnetic moment per hole around 1–1.4 ML, which is related to a magnetic phase transition of the γ-Fe as we will discuss in the next section.

IV. DISCUSSION

Modifications in the film morphology and the film structure usually have strong influences on the magnetic moments. We have already shown that the fcc to bcc phase transformation results in an increase of both m_{orb}/N_h and m_{spin}/N_h towards their bulk values. On the other hand, the increase of m_{orb} at very low coverage is more likely to be due to size effects. Indeed, it is well known that a more atomiclike structure, such as a surface or a cluster, leads to a narrowing of the $3d$ band which enhances the orbital moment.[29] Ascribing the increase of m_{orb} to the edge atoms, we use a simple model for the island growth: rectangular islands with only the length l increasing during the growth, the width w is assumed to be constant in our approximation. In this model the number of edge atoms is proportional to $l+w$ and the number of surface atoms to lw. We deduce a factor ~50 between m_{orb} for the edge atoms and m_{orb} for the surface atoms, i.e., $m_{\text{orb}}^{\text{edge}}\approx 0.5\mu_B$. This result is reasonable as for a free Fe atom $m_{\text{orb}}=2\mu_B$. This behavior has been experimentally observed in several systems.[30]

Since the anisotropy is correlated to the orbital magnetic moment, it also shows an increase below ~1.2 ML. Bruno has demonstrated[26] in a perturbation picture that for $3d$ metals the anisotropy energy is proportional to the anisotropy of the orbital moment. If we use our values of $(m_{\text{orb}}^{\perp}-m_{\text{orb}}^{\parallel})$ to make a rough estimation of the anisotropy energy using Bruno's formalism, we obtain -0.6 meV/atom for the lowest coverage, which is in very good agreement with Bruno's calculation for an Fe fcc(111) layer giving -0.61 meV/atom.[26] If we go to higher coverages just below the 2D percolation, this value goes down to -0.2 meV/atom, which can be explained by the relative decrease of the atomic sites with lowest coordination with increasing coverage.[31]

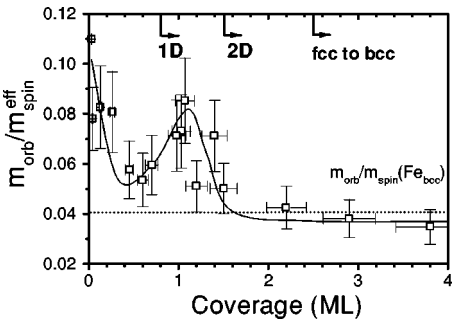

FIG. 7. $m_{\text{orb}}/m_{\text{spin}}^{\text{eff}}$ as a function of the coverage. The solid line is a guide for the eye. The arrows on the top scale at 0.8, 1.5, and 2.5 ML correspond, respectively, to the approximate coverage where the Fe starts to coalesce into 1D wire, reaches the 2D percolation, and undergoes the fcc to bcc phase transformation. (All the measurements have been performed below the blocking temperature with a magnetic field sufficient to saturate the sample.)

We now discuss the behavior of the spin magnetic moment below 2 ML. Indeed, despite the uncertainty in the determination of both the moment and the thickness, two different regions can be clearly identified on either side of 0.8 ML, which correspond to the coalescence of the islands into 1D stripes. It is important to note that this effect is also seen in the ratio $R=m_{\text{orb}}/m_{\text{spin}}^{\text{eff}}$ as shown in Fig. 7. This type of analysis, which is less sensitive to errors, confirms the results of Fig. 6. However, it is more difficult to interpret as the variations of m_{spin} and m_{orb} are no longer separable. According to Fig. 6, below 0.8 ML $m_{\text{spin}}/N_h \approx (0.40\pm 0.05)\mu_B$ per hole and above this coverage $m_{\text{spin}}/N_h\approx(0.20\pm 0.05)\mu_B$ per hole until the bcc phase starts to appear at ~1.8 ML. If we want more quantitative values for the magnetic moment, we have to assume a number of holes, N_h, in the $3d$ band. For bulk bcc Fe, an average of different band-structure calculations gives $N_h=3.39$.[27,32,33] If we suppose some charge transfer from the Fe to the Cu, induced by the fcc structures or the cluster morphology, then we can reasonably say that this should not exceed 0.5 holes. Usually the theory predicts an increase of N_h towards the surface as it is more atomiclike,[27] but XAS experiments on Ni/Cu(001) found a decrease of ~0.5 holes[21] and likewise theoretical work[33] predicts a very small decrease (~1%) for Fe-Cu multilayers. In summary, we can assume that the number of holes is equal to 3.4 with an uncertainty of 15%. With this value we can now say that for a coverage $d<0.8$ ML, $m_{\text{spin}}=(1.4\pm 0.2)\mu_B$ and for $0.8\text{ ML}<d<\sim 1.5$ ML, $m_{\text{spin}}=(0.7\pm 0.2)\mu_B$. The latter value is consistent with previous measurements using a torsion magnetometer on copper capped Fe/Cu(111) (Ref. 34) films $(0.58\pm 0.13\mu_B)$ and the work of Shen *et al.*[2,3] To our

knowledge, $m_{spin}=(1.4\pm0.2)\mu_B$ has only been measured for γ-Fe in a Cu(10 Å)/Fe(0–35 Å)/Ni(50 Å) wedged sample.[35] In this work a spin phase transition is observed for an Fe thickness of 10 Å, and it is also ascribed to a change in the fcc crystallographic structure.

If we look at the calculations of the magnetic phase diagram versus the lattice parameter (see, for instance, Refs. 5–7), they all predict, among others, ferromagnetic phases with different high-spin and low-spin values. Using the results of these theoretical models, if we suppose that the Fe overlayer assumes the lattice parameter of fcc Cu ($a_{Cu}=3.61$ Å) or of bulk fcc Fe ($a_{Fe}=3.59$ Å), we find two kinds of low-spin magnetic moments, with values of $\sim1.5\mu_B$ and $\sim0.4\mu_B$, respectively. So one can imagine that at the very beginning of the growth, when the deposit essentially forms monolayer islands, Fe assumes exactly the lattice parameter of the Cu substrate, i.e., 3.61 Å, with $m_{spin}\sim1.5\mu_B$. However, once the islands start to coalesce to form the 1D stripe, the strain is relaxed. When this coalescence is complete, at (0.8 ± 0.1) ML, the whole Fe film assumes its equilibrium fcc atomic volume, i.e., $a_{Fe}=3.59$ Å, resulting in a lower value of m_{spin}. This proposed structural relaxation could be sufficient to drive the observed change in the magnetic spin moment. Similar behavior has already been observed in the case of Fe films deposited on Cu(111) by PLD, with a phase transition at ~3 ML.[8,9] Indeed, this evaporation technique allows one to grow fcc Fe in a high-spin phase [while Fe/Cu(111) obtained by TD is usually low-spin], which is explained by a slightly enlarged lattice parameter compared to films produced by TD. This structural difference is underlined by electron diffraction. In our case, however, further investigations of the possible structural change are limited as the modifications of the lattice parameter are expected to be small (~0.5)% and the coverages are so low that only grazing incidence x-ray diffraction might be able to reveal the structural changes.

V. CONCLUSIONS

Using XMCD we are able to investigate the quantitative magnetic properties of Fe nanostructures deposited on a vicinal Cu(111) substrate. We extend the understanding of this system to the very low coverage range and confirm the out-of-plane anisotropy even for very small clusters. In the same way we find the expected increase of the anisotropy energy below ~1.5 ML and our estimated values are very close to the ones predicted by theoretical predictions. The most striking result is the observation of two low-spin phases below and above 0.8 ML, corresponding to the coverage at which coalescence of the clusters into 1D stripes is observed. These two magnetic phases are tentatively ascribed to structural changes during coalescence. The Fe clusters, which are purely pseudomorphic at low coverage, undergo a strain relaxation so that the lattice parameter approaches the stable fcc Fe value.

ACKNOWLEDGMENTS

The authors are grateful to K. Larsson for his invaluable technical assistance and S. Decossas for providing us with the AFM results. We also want to thank S. S. Dhesi for his useful comments on the manuscript. P.O. would like to acknowledge F. Scheurer, H. Bulou, and S. Padovani for stimulating discussions.

[1] See, for instance, M. T. Kief and W. F. Egelhoff, Jr., Phys. Rev. B **47**, 10 785 (1993); D. Tian, F. Jona, and P. M. Marcus, *ibid.* **45**, 11 216 (1992).

[2] J. Shen, R. Skomski, M. Klaua, H. Jenniches, S. Sundar Manoharan, and J. Kirschner, Phys. Rev. B **56**, 2340 (1997).

[3] J. Shen, M. Klaua, P. Ohresser, H. Jenniches, J. Barthel, Ch. V. Mohan, and J. Kirschner, Phys. Rev. B **56**, 11 134 (1997).

[4] J. Dorantes-Dávila and G. M. Pastor, Phys. Rev. Lett. **81**, 208 (1998).

[5] V. L. Moruzzi, P. M. Marcus, and J. Kübler, Phys. Rev. B **39**, 6957 (1989).

[6] Yu-mei Zhou, Wen-qing Zhang, Lie-ping Zhong, and Ding-sheng Wang, J. Magn. Magn. Mater. **145**, L273 (1995).

[7] E. G. Moroni, G. Kresse, J. Hafner, and J. Furthmüller, Phys. Rev. B **56**, 15 629 (1997).

[8] J. Shen, P. Ohresser, Ch. V. Mohan, M. Klaua, J. Barthel, and J. Kirschner, Phys. Rev. Lett. **80**, 1980 (1998).

[9] P. Ohresser, J. Shen, J. Barthel, M. Zheng, Ch. V. Mohan, M. Klaua, and J. Kirschner, Phys. Rev. B **59**, 3696 (1999).

[10] See, for instance, P. Ohresser, F. Scheurer, B. Carrière, J. P. Deville, and A. Dobroiu, Surf. Sci. **352-354**, 567 (1996); F. Scheurer, P. Ohresser, H. Bulou, J. P. Deville, B. Carrière, and A. Dobroiu, Phys. Rev. B **56**, 13 490 (1997).

[11] S. Müller, P. Bayer, C. Reischl, K. Heinz, B. Feldmann, H. Zillgen, and M. Wuttig, Phys. Rev. Lett. **74**, 765 (1995).

[12] J. G. Tobin, G. D. Waddill, A. F. Jankowski, P. A. Sterne, and D. P. Pappas, Phys. Rev. B **52**, 6530 (1995); J. Hunter Dunn, D. Arvanitis, and N. Mårtensson, *ibid.* **54**, R11 157 (1996); D. Schmitz, C. Charton, A. Scholl, C. Carbone, and W. Eberhardt, *ibid.* **59**, 4327 (1999).

[13] B. T. Thole, P. Carra, F. Sette, and G. van der Laan, Phys. Rev. Lett. **68**, 1943 (1992).

[14] P. Carra, B. T. Thole, M. Altarelli, and X. Wang, Phys. Rev. Lett. **70**, 694 (1993).

[15] A. Brodde, K. Dreps, J. Binder, Ch. Lunau, and H. Neddermeyer, Phys. Rev. B **47**, 6609 (1993); M. Klaua, H. Höche, H. Jenniches, J. Barthel, and J. Kirschner, Surf. Sci. **381**, 106 (1997).

[16] See, for instance, S. Sundar Manoharan, M. Klaua, J. Shen, J. Barthel, H. Jenniches, and J. Kirschner, Phys. Rev. B **58**, 8549 (1998).

[17] V. Chakarian, Y. U. Idzerda, and C. T. Chen, Phys. Rev. B **57**, 5312 (1998).

[18] C. T. Chen, Y. U. Idzerda, H.-J. Lin, N. V. Smith, G. Meigs, E. Chaban, G. H. Ho, E. Pellegrin, and F. Sette, Phys. Rev. Lett. **75**, 152 (1995).

[19] The background correction treatment is similar to the one used in Chen *et al.*[18] First, a flat baseline is removed, with a slope given by the preedge absorption cross section. To subtract the transitions into the continuum states we use a two-step function aligned at the maxima of the L_3 and L_2 edges with a relative

ratio of 2:1, which is the expected intensity ratio for transitions into the two continua. The slope of this step function is extrapolated from the average slope of the absorption cross section 15 eV after the L_2 edge and over ~30 eV energy range. Different refinements can be added to this method (for instance, smoothing of the step function) but this does not change the overall results.

[20] R. Nakajima, J. Stöhr, and Y. U. Idzerda, Phys. Rev. B **59**, 6421 (1999).

[21] As a remark, we want to add that some groups use the white line intensity as a probe for N_h as this value is proportional to the unoccupied $3d$ states: see, for instance, P. Srivastava, N. Haack, H. Wende, R. Chauvistré, and K. Baberschke, Phys. Rev. B **56**, R4398 (1997); S. S. Dhesi, H. A. Dürr, G. van der Laan, E. Dudzik, and N. B. Brookes, *ibid.* **60**, 12 852 (1999). However, in the case of a dilute system, i.e., a submonolayer, this method is very sensitive to any nonlinearity, as we will demonstrate in a forthcoming paper.

[22] H. A. Dürr, S. S. Dhesi, E. Dudzik, D. Knabben, G. van der Laan, J. B. Goedkoop, and F. U. Hillebrecht, Phys. Rev. B **59**, R701 (1999).

[23] E. Dudzik, H. A. Dürr, S. S. Dhesi, G. van der Laan, D. Knabben, and J. B. Goedkoop, J. Phys.: Condens. Matter **11**, 8445 (1999).

[24] H. Takeshita, Y. Suzuki, H. Akinaga, W. Mizutani, K. Ando, T. Katayama, A. Itoh, and K. Tanaka, J. Magn. Magn. Mater. **165**, 38 (1997).

[25] S. Padovani, I. Chado, F. Scheurer, and J. P. Bucher, Phys. Rev. B **59**, 11 887 (1999).

[26] P. Bruno, Phys. Rev. B **39**, 865 (1989).

[27] R. Wu and A. J. Freeman, Phys. Rev. Lett. **73**, 1994 (1994).

[28] J. Stöhr and H. König, Phys. Rev. Lett. **75**, 3748 (1995).

[29] D. Weller, J. Stöhr, R. Nakajima, A. Carl, M. G. Samant, C. Chappert, R. Mégy, P. Beauvillain, P. Veillet, and G. A. Held, Phys. Rev. Lett. **75**, 3752 (1995).

[30] See, for instance, P. Srivastava, F. Wilhelm, A. Ney, M. Farle, H. Wende, N. Haack, G. Ceballos, and K. Baberschke, Phys. Rev. B **58**, 5701 (1998).

[31] F. Bodker, S. Morup, and S. Linderoth, Phys. Rev. Lett. **72**, 282 (1994).

[32] R. Wu, D. Wang, and A. J. Freeman, Phys. Rev. Lett. **71**, 3581 (1993).

[33] G. Y. Guo, H. Ebert, W. M. Temmerman, and P. J. Durham, Phys. Rev. B **50**, 3861 (1994).

[34] W. Kümmerle and U. Gradmann, Phys. Status Solidi A **45**, 171 (1978).

[35] J. Stöhr and R. Nakajima, J. Phys. (Paris), Colloq. **7**, C2-47 (1997); J. Stöhr and R. Nakajima, IBM J. Res. Dev. **42**, 73 (1998).